metals

MDPI

Article

Corrosion and Formation of Surface Films on AZ31 Mg Alloy in Aqueous Solution Containing Sulfate Ions with Different pHs

Duyoung Kwon [1,2], Hien Van Pham [1,3], Pungkeun Song [2,*] and Sungmo Moon [1,2,*]

[1] Nano-Surface Materials Division, Korea Institute of Materials Science, Changwon 51508, Republic of Korea; legel@kims.re.kr (D.K.); phamvanhien@kims.re.kr (H.V.P.)
[2] Department of Materials Science and Engineering, Pusan National University, Busan 46241, Republic of Korea
[3] Advanced Materials Engineering, University of Science and Technology, Daejeon 34113, Republic of Korea
* Correspondence: pksong@pusan.ac.kr (P.S.); sungmo@kims.re.kr (S.M.)

Abstract: This study aims to clarify how a solution's pH can influence the corrosion and formation of surface films on the AZ31 Mg alloy in aqueous solutions containing sulfate ions. The corrosion and surface film formation behaviors were examined using in situ observation, open-circuit potential (OCP) transient, weight change measurement and electrochemical impedance spectroscopy (EIS). The morphologies of the surface films were analyzed via metal/insulator/metal (MIM) coloring and FESEM. The findings show that at pH 2, severe corrosion occurred together with rapid hydrogen evolution and formation of a highly porous surface film with numerous cracks. However, at pH 3, the corrosion rate dropped significantly and remarkably low corrosion rates were observed at pH 4 and 10. At pH 11 and 12, weight gains were noticed, suggesting the growth of surface films on the AZ31 Mg alloy. Flake-like films formed at pH 12, while needle-like structures were present between pH 3 and 11. Impedance measurements revealed increased impedance at higher pH of sulfate-ion-containing solutions. Higher impedance was related to the formation of denser surface films on the AZ31 Mg alloy. In addition, the films displayed metal/insulator/metal (MIM) colors via Au coating above pH 4, indicating uniform film thickness despite the presence of needle-like or flake-like structures.

Keywords: AZ31 Mg alloy; pH effect; corrosion; surface film; sulfate ion

Citation: Kwon, D.; Pham, H.V.; Song, P.; Moon, S. Corrosion and Formation of Surface Films on AZ31 Mg Alloy in Aqueous Solution Containing Sulfate Ions with Different pHs. *Metals* **2023**, *13*, 1150. https://doi.org/10.3390/met13071150

Academic Editors: Guosong Wu, Jiapeng Sun and Hao Wu

Received: 28 May 2023
Revised: 16 June 2023
Accepted: 20 June 2023
Published: 21 June 2023

1. Introduction

Magnesium (Mg) and its alloys have attracted much attention as lightweight materials for the aerospace, automobile, biomedical and electronics industries due to their low density of 1.74 g·cm^{-3} compared with other structural materials such as steel (7.85 g·cm^{-3}), titanium (4.5 g·cm^{-3}) and aluminum (2.7 g·cm^{-3}) [1–4]. AZ31 is one of the most widely used magnesium alloys, containing approximately 3% aluminum (Al) and 1% zinc (Zn). The addition of aluminum and zinc enhances the strength, hardness, creep resistance, castability and weldability. However, the addition of aluminum leads to the formation of intermetallic compounds such as $Mg_{17}Al_{12}$ and Mg_2Al_3 in the Mg matrix, accelerating corrosion due to a micro-galvanic coupling effect between the intermetallic compounds and the matrix [5,6]. It is a serious drawback to their use in a wide range of industrial applications [7,8].

Mg corrosion in aqueous environments refers to the degradation process of Mg or its alloys when they are exposed to water or water-containing environments [9]. This process is electrochemical in nature and is accelerated by the presence of water, due to high chemical reactivity of magnesium. When Mg comes into contact with water, magnesium oxide (MgO) and magnesium hydroxide ($Mg(OH)_2$) layers are spontaneously formed on the surface [10–12]. Moreover, when Mg is exposed to an environment containing CO_2, $Mg(OH)_2$ can further react to form a magnesium carbonate ($MgCO_3$) layer [13,14]. These

layers of MgO, $Mg(OH)_2$ and $MgCO_3$ are easily broken in aqueous environments containing chloride ions (Cl^-), sulfate ions (SO_4^{2-}) or acidic solutions [15,16]. In previous studies, Mg corrosion caused by Cl^- ions was reported to occur due to the disruption of the surface oxide/hydroxide layers ($MgO/Mg(OH)_2$) [17–19] and the formation of a water-soluble $MgCl_2$ layer caused by reaction with Mg^{2+} ions [20–22]. Samaniego et al. have reported that the electron released from the dissolution of Mg can be utilized to reduce sulfate ions (SO_4^{2-}) to sulfur dioxide (SO_2) on the Mg surface. These reduced ionic species could affect the corrosion behavior and formation of surface film on Mg alloys [23]. SO_4^{2-} ions are also known to form soluble magnesium sulfate ($MgSO_4$) in aqueous solutions [24,25].

We have reported the effects of chloride ion (Cl^-), sulfate ion (SO_4^{2-}), phosphate ion (PO_4^{3-}) and fluoride ion (F^-) in neutral aqueous solutions on the electrochemical and corrosion properties of the AZ31 Mg alloy [26,27]. An interesting aspect among the experimental findings was that no weight change was observed in the AZ31 Mg alloy during immersion in a neutral aqueous solution containing sulfate ions. This was considered to be due to the formation of a dense and protective surface film in the aqueous neutral solution. The corrosion behavior of Mg and its alloys is largely affected by the solution's pH [28,29]. In general, H^+ ions can dissolve the surface oxide films and readily participate in the cathodic reduction reaction, thereby accelerating the overall corrosion reaction. In contrast, the corrosion rate of Mg and its alloy can be relatively low due to the formation of a protective layer of magnesium hydroxide ($Mg(OH)_2$). However, the effects of the solution's pH on corrosion and surface film formation on AZ31 Mg alloy has not been reported in the presence of sulfate ions in an aqueous solution.

In this work, to investigate the effect of the pH of an aqueous solution containing sulfate ions (SO_4^{2-}) on the corrosion and formation of a surface film on AZ31 Mg alloy surface, we prepared SO_4^{2-} ion-containing aqueous solutions with pHs of 2, 3, 4, 10, 11 and 12 by adding a 10 M NaOH solution to a 0.1 M H_2SO_4 solution. The corrosion and formation behaviors of the surface films was investigated through in situ observation, open-circuit potential (OCP) measurements, weight loss/gain measurements, and electrochemical impedance spectroscopy (EIS). The surface colors of the specimen after 30 min of immersion were observed before and after Au coating, and the morphologies of the surface films formed during immersion for 30 min were analyzed using a field emission-scanning electron microscope (FESEM).

2. Materials and Methods

2.1. Sample Preparation

The commercial AZ31B Mg alloy plate (wt.% Al 2.94, Zn 0.8, Mn 0.3, Si < 0.1, Fe < 0.005, Cu < 0.05, Mg balance, POSCO, Republic of Korea) was used for this work. The Mg plate was polished from 220 grit to 4000 grit using SiC abrasive papers with ethyl alcohol and then masked using a polyester tape, exposing a circular area of 1.3 cm^2. A copper wire was connected to the backside of specimens for electrical connection and the contact resistance between the copper wire and the Mg plate was verified to be less than 0.5 mΩ.

2.2. In Situ Observation and Weight Change

In situ observation of the AZ31 Mg alloy specimen surface was conducted during immersion for 30 min in 1 L of 0.1 M H_2SO_4 solutions with pHs ranging from 2 to 12 at 20 ± 0.5 °C without agitating. The pH of the solution was adjusted by adding small amounts of the 10 M NaOH solution. The AZ31 Mg alloy specimen surface was photographed during immersion using a digital camera under a consistent illumination condition. The weight of the AZ31 Mg alloy plate specimen with surface area of approximately 46 cm^2, was measured before and after 30 min of immersion using a balance (METTLER TOLEDO, XPE205V, Columbus, OH, USA). The weight changes were calculated by subtracting the initial weights before immersion from those measured after immersion.

2.3. Electrochemical Measurements

Open-circuit potential (OCP) and electrochemical impedance spectroscopy (EIS) measurements were conducted using an electrochemical workstation (Biologic, VMP3 multichannel potentiostat, France). The typical three-electrode system consisting of a working electrode, a counter electrode (Pt mesh) and a reference electrode (Ag/AgCl electrode) was employed for electrochemical measurements. After immersing the specimens for 30 min, EIS measurements were performed over a frequency range of 10^5 to 10^{-1} Hz, with a signal amplitude of 10 mV. The obtained EIS results were fitted with EC-Lab software using equivalent circuit models, as suggested in a previous paper [26]. Both the OCP and the EIS measurements were repeated three times to ensure reproducibility.

2.4. MIM Coloring and Surface Morphologies Observation

Metal/insulator/metal (MIM) coloring was achieved by depositing a gold coating layer using sputter coater (Ted Pella, 108 Auto Sputter Coator, United States) on the AZ31 Mg alloys after immersion for 30 min in 0.1 M H_2SO_4 solutions with different pHs. The gold-coated surfaces were photographed using a digital camera under the same illumination conditions. The surface morphologies were observed using a field emission scanning electron microscopy (JEOL, JSM-7900F, Japan).

3. Results and Discussion

3.1. In Situ Observations of the AZ31 Mg Alloy Surfaces during Immersion

Figure 1 shows the changes in gas evolution behavior with an immersion time of up to 30 min on the AZ31 Mg alloy surface in SO_4^{2-} ion-containing aqueous solutions with different pHs. The specimens were set vertically so that gas bubbles moved upwards on the specimen surface. Two different gas evolution behaviors were observed. One is the formation of large-sized bubbles at the same site, which were finally detached from the surface after growing to a certain size. This type of bubbles was found at all pHs, from 2 to 12. The other type is the continuous formation and detachment of small-sized bubbles at the same site in which the bubble lines were formed, as can be seen at pHs lower than 4 and higher than 10 (Figure 1a,b,e,f). The line of gas bubbles on the vertically set Mg alloy sample was reported to result from a continuous generation of hydrogen bubbles in impurities containing Fe, Ni or Cu [30].

At pH 2, vigorous hydrogen evolution was observed immediately after immersion in the SO_4^{2-} ion-containing aqueous solution (Figure 1a), and its rate decreased with increasing immersion time, as shown in the magnified images (Figure 1(a1–a5)). It is noticed that the surface color of the specimen changed from dark to bright (Figure 1a only at pH 2). Considering that the light comes from the upper site, it is readily inferred that the brightened surface of the specimen after immersion for more than 10 min is due to an increased reflection of diffused light from the rough surface obtained at pH 2. In contrast, dark surfaces of the specimen obtained at pHs ranging from 3 to 12 could reveal the relatively smooth surface, indicating a low corrosion rate at pHs from 3 to 12.

At pHs 3, 11 and 12 of the SO_4^{2-} ion-containing aqueous solution, two types of gas evolution behavior of a large-sized bubble formation and continuous evolution of small-sized bubbles, showing a line of gas bubbles, were observed. The number of large-sized gas bubbles decreased with increasing immersion time at pHs lower than 11. At pH 12 of the SO_4^{2-} ion-containing aqueous solution, however, the number of large-sized gas bubbles did not decrease significantly and the bubble size increased slightly with increasing immersion time. At pHs 4 and 10 of the SO_4^{2-} ion-containing aqueous solution, no line of gas bubbles was observed during immersion. At present, the reason why no line of gas bubbles was observed at pHs 4 and 10 is not clearly understood and needs to be studied by considering the absence and presence of impurity particles and the fast passivation of the area surrounding impurity particles.

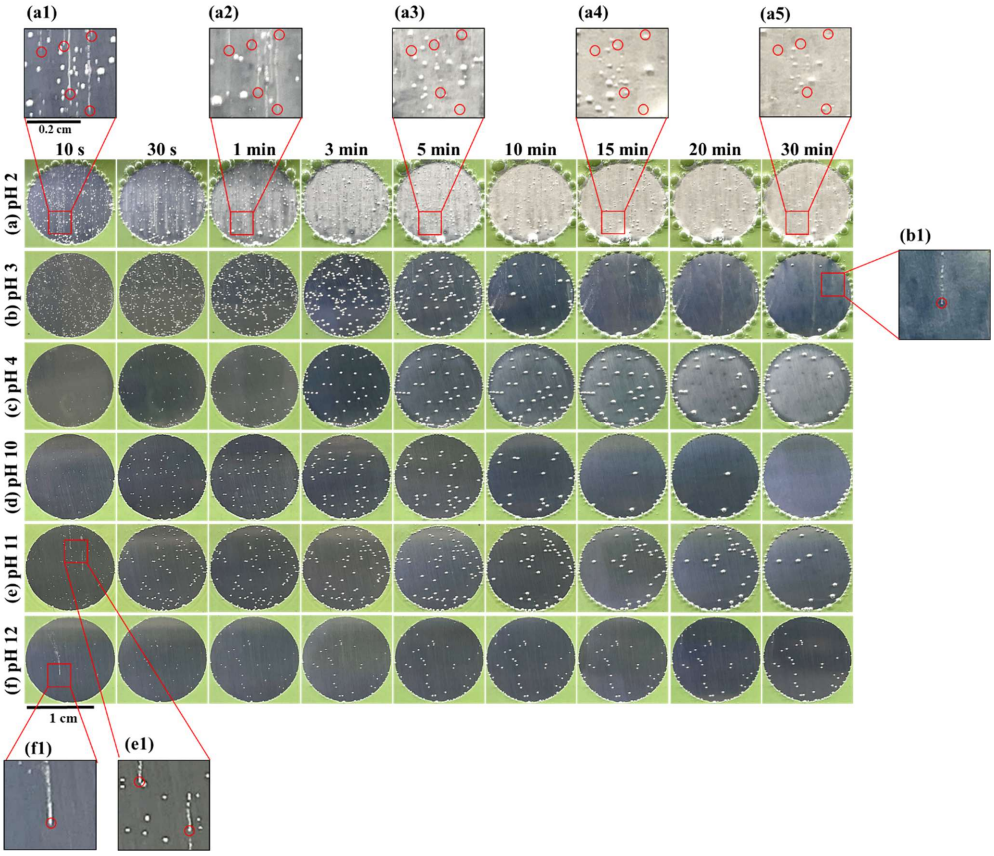

Figure 1. Photographs of AZ31 Mg alloy surface during immersion in sulfate ion-containing aqueous solutions with pH of (**a**) 2, (**b**) 3, (**c**) 4, (**d**) 10, (**e**) 11 and (**f**) 12. The solutions pH was adjusted by adding 10 M NaOH solution into 0.1 M H_2SO_4 solution and a1~f1 are the magnified images of the specimen surface where bubbles are generated.

3.2. Open-Circuit Potential Transients

Open-circuit potential (OCP) transients of AZ31 Mg alloys during 30 min of immersion in SO_4^{2-} ion-containing aqueous solutions with different pHs are presented in Figure 2. The OCP increased rapidly with time in the initial stage of immersion up to approximately 60 s and then slowly increased for 30 min irrespectively of the pH of the solutions. The rapid OCP increase in the early stage of immersion is attributed to the formation of stable surface films on the AZ31 Mg alloy surface in SO_4^{2-} ion-containing aqueous solutions. The slow increase in OCP after approximately 60 s, without reaching a steady state, reveals that the electrochemical anodic reaction rate is slowed down with immersion time, suggesting the growth of stable oxide films with immersion time on the AZ31 Mg alloy surface. The growth of stable oxide films with immersion time has been reported to result in an increase in the OCP of Mg alloys [31].

The OCP values of the AZ31 Mg alloy obtained after immersion for 30 min showed largely decreased values in highly acidic solutions of pH 2 and slightly decreased values in alkaline solutions of pH 10~12, as shown in Figure 3. The largely decreased OCP value at pH 2 of the SO_4^{2-} ion-containing aqueous solution seems to result from the fast anodic dissolution of AZ31 Mg alloy, as experimentally verified via the high gas evolution rate shown in Figure 1a. The slightly decreased OCP values in alkaline solutions compared to neutral solutions are attributable to a decreased cathodic reaction with the solution's increasing pH. In addition, the presence of SO_4^{2-} ions in the aqueous solution may influence the OCP of the Mg alloy because sulfate ions can form MgO and $Mg(OH)_2$ together with various complexes of $(MgCO_3)_4{\cdot}Mg(OH)_2{\cdot}4H_2O$ and $Mg(OH)_2{\cdot}2MgSO_4$ by reacting with Mg^{2+} ions on the Mg alloy surface [32,33]. However, the detailed mechanism of these

interactions and their influence on OCP is not clear; therefore, additional investigations are necessary.

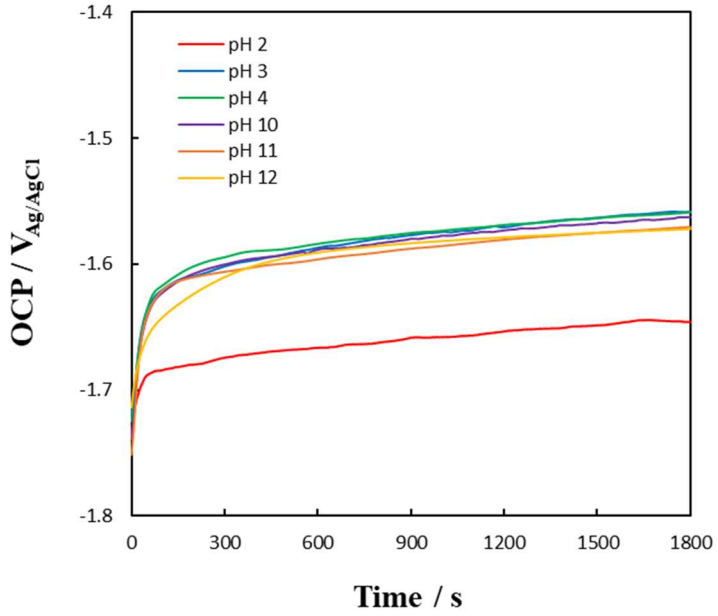

Figure 2. Open-circuit potential transients of AZ31 Mg alloy during immersion in sulfate ion−containing aqueous solutions with different pHs. The solutions pH was adjusted to 2, 3, 4, 10, 11 and 12 by adding 10 M NaOH solution into 0.1 M H_2SO_4 solution.

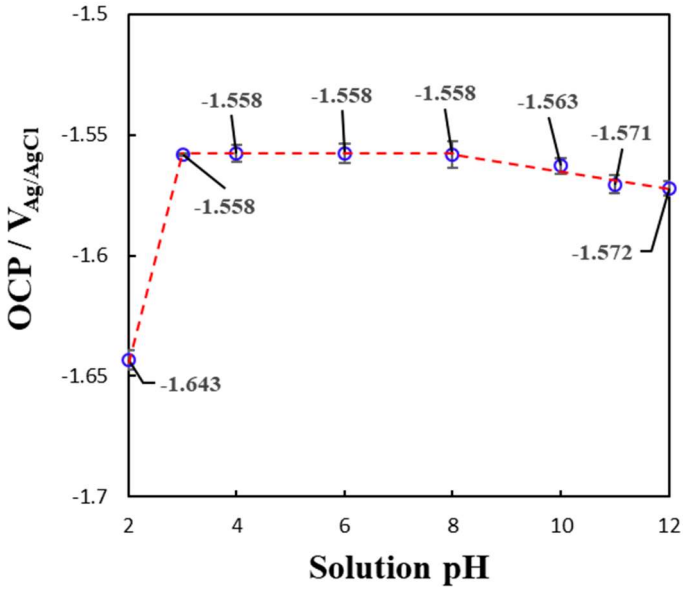

Figure 3. Plot of open-circuit potential of AZ31 Mg alloy obtained at 30 min of immersion versus pH of sulfate ion−containing aqueous solutions.

3.3. Weight Loss and Gain

The weight changes of AZ31 Mg alloy after immersion for 30 min in SO_4^{2-} ion-containing aqueous solutions with different pHs are plotted as a function of the solution's pH in Figure 4. An extremely large weight loss rate of approximately −39.099 μg/cm^2·min was obtained at pH 2, indicating severe corrosion of the AZ31 Mg alloy. The weight loss became very small at pHs 3, 4 and 10, which could be related to the formation of stable dense surface oxide films on the AZ31 Mg alloy surface. Interestingly, the weight loss rate decreases by approximately 80 times as the solution's pH increases from 2 to 3. This

suggests that hydrogen ions (H^+) are readily reduced to hydrogen gas and thus act as an oxidizer, which facilitates anodic reactions of metal. As the pH of an aqueous solution increases to more than 3, anodic oxidation of metal is significantly reduced, as manifested by the low weight loss shown in Figure 4. The formation of stable and protective surface films would effectively protect from further corrosion of AZ31 Mg. Thus, it could reduce the weight loss.

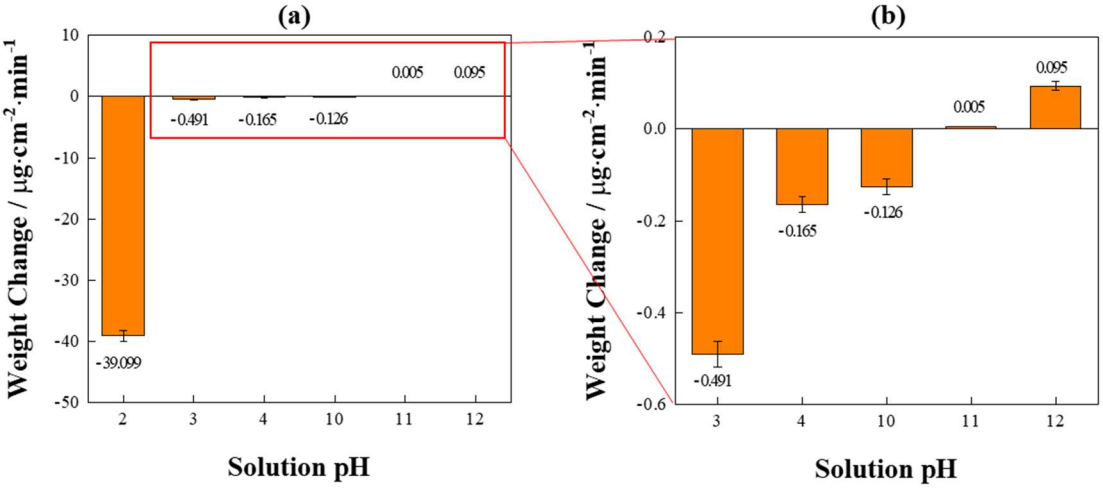

Figure 4. Weight changes of the AZ31 Mg alloy specimen after immersion for 30 min in sulfate ion−containing aqueous solutions with different pHs: (**a**) pH 2, 3, 4, 10, 11 and 12; (**b**) pH 3, 4, 10, 11 and pH 12. The solutions pH was adjusted by adding 10 M NaOH solution into 0.1 M H_2SO_4 solution.

Interestingly, weight gain rates of 0.005 μg/cm^2·min and 0.095 μg/cm^2·min were obtained in sulfate-ion-containing aqueous solutions at pH 11 and 12, respectively. These could be due to the growth of protective surface films on the AZ31 Mg alloy surface. The formation and growth behavior of surface oxide films with immersion time of more than 30 min at pH 12, and the growth behavior of surface oxide films in more alkaline solutions will be discussed in a future paper.

3.4. Electrochemical Impedance Spectroscopy

Figure 5 shows bode plots and Nyquist plots obtained from the AZ31 Mg alloy at open-circuit potential in sulfate ion-containing aqueous solutions with different pHs after immersion for 30 min. In the bode plot (Figure 5a), the impedance of the AZ31 Mg alloy in the low frequency region increased largely, by one order of magnitude, when the solution's pH increased from pH 2 to pH 3 and from pH 11 to pH 12. The large increase in the impedance between pH 2 and pH 3 is attributable to slowed corrosion, as shown in Figure 4a, and the increase in impedance between pH 11 and pH 12 could be due to the formation of resistive surface films, as can be inferred from the weight increase in the specimen after the immersion experiment (Figure 4b).

At pH 12 of the SO_4^{2-} ion-containing aqueous solution, the Nyquist plot was characterized by the largest capacitive semicircle. At a pH lower than 11, two capacitive semicircles were identified in the high-to-medium and low-frequency regions. An additional inductive loop appeared only at pH 2. The diameter of the capacitive semicircle in the high-frequency region increased with the increasing pH of the sulfate-ion-containing aqueous solutions. Interestingly, the peak frequencies of the capacitive semicircle in the high-frequency region decreased as the pH of the solution increased. This indicates an increase in the RC time constant caused by an increased surface film resistance, which is consistent with a decreased corrosion rate of the AZ31 Mg alloy as the pH increases, as shown in Figure 4.

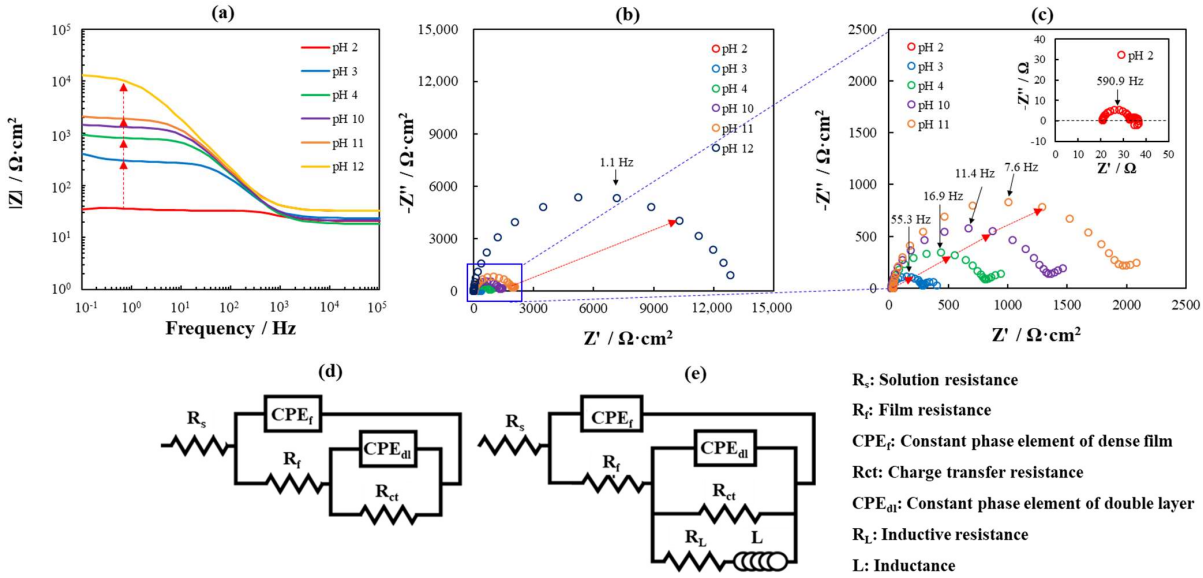

Figure 5. (**a**) Bode plots, (**b**,**c**) Nyquist plots obtained from the AZ31 Mg alloy in sulfate ion−containing aqueous solutions with different pHs, and (**d**,**e**) equivalent circuits used for fitting the impedance data.

The Nyquist plots in Figure 5 were fitted using the equivalent circuits suggested in previous studies [26]. The resistance and capacitance values of the porous and dense surface films obtained are shown in Figure 6 as a function of the pH of the solution. In acidic solutions with pHs ranging from 2 to 4, the resistance of the porous film increased largely with the increasing pH, which suggests that the surface film becomes less permeable to ions, likely due to t formation of thicker or denser surface films. A decreased capacitance of the surface films with the increasing pH in Figure 6 supports the thickening of the surface films. Both the film resistance and capacitance values reported in near neutral solutions [27] were very close to those obtained in this study at pH 4 and pH 10, suggesting that film resistance and capacitance are not significantly changed with pHs between 4 and 10. In contrast, in alkaline conditions above pH 10, these became more pronounced. In conclusion, it can be said that the surface films formed on AZ31 Mg alloy are denser and thicker with the increasing solution's pH, which effectively serves as a barrier against corrosion.

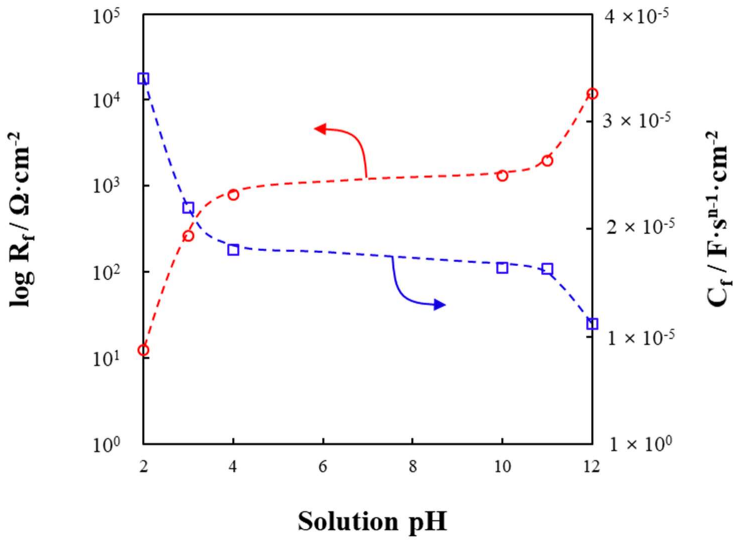

Figure 6. Plots of resistance and capacitance of surface film on AZ31 Mg alloy obtained by fitting EIS data of Figure 5 vs. solution's pH.

3.5. Surface Appearance

Figure 7 exhibits the surface colors of the AZ31 Mg alloy surface obtained after 30 min of immersion in sulfate-ion-containing aqueous solutions with various pH values before and after Au coating via sputtering. After Au coating, various colors ranging from yellow to blue were observed on the specimen surface due to optical interference caused by the metal/insulator/metal (MIM) structure [34].

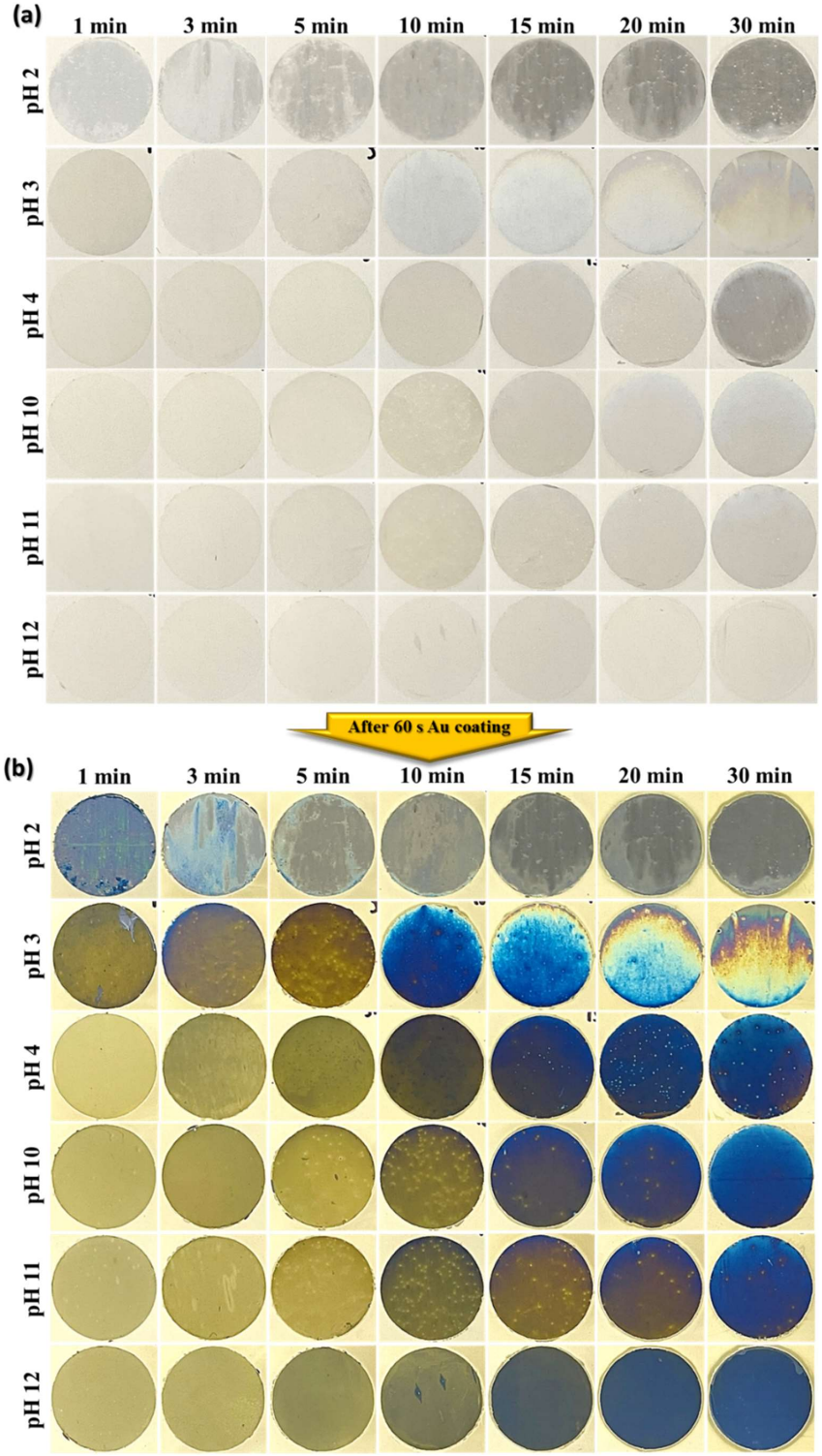

Figure 7. Photographs (**a**) before and (**b**) after Au coating of the AZ31 Mg alloy surfaces which were immersed for 30 min in sulfate-ion-containing aqueous solutions with different pHs.

At pH 2, the specimen surface immersed for 1 min displayed a uniform white color, and after immersion for more than 3 min, the surface color became darker with immersion time. The darkened surface with immersion time seems to arise from the formation of porous films and increased surface roughness due to corrosion, as revealed in Figures 1 and 4. After Au coating, an interference color caused by MIM structure was observed only on the surface immersed for less than 3 min at pH 2 (Figure 7b). On the surfaces of the specimen immersed for more than 3 min, no interference colors appeared. This reveals that a uniform and thin surface film is formed only in the early stage of immersion in a pH 2 solution.

At pH 3, the surface color after 1 min of immersion before Au coating was dark; then, it became brighter with increasing the immersion time up to 15 min, after which the upper surface became darkened. The dark surface after 1 min of immersion seems to be related to fast corrosion, as manifested by vigorous gas evolution, as shown in Figure 1. The surface color after Au coating was yellow up to 5 min of immersion, and it changed into blue after 10 m of immersion. Irregular surface colors of the specimens appeared when immersed for more than 15 min. Various colors of AZ31 Mg alloy obtained via surface reactions in sulfate ion-containing aqueous solution, primarily a mixture of yellow and blue arising from the MIM structure, may be attributed to differences in the thickness and composition of surface films. Further research is necessary to understand the relationship between surface film properties and interference color.

At pH 4~12, the surface color of the AZ31 Mg alloy was relatively uniform and it became darker with immersion time (Figure 7a); in addition, the interference colors after Au coating changed from yellow to blue with immersion time (Figure 7b). The uniform surface color for pH values higher than 4 can be attributed to the uniform thickness of the surface film formed on the AZ31 Mg alloy surface during immersion. As the immersion time increased, the surface color shifted towards a deeper blue color, which may indicate the growth of the surface film. The growth of the surface film with immersion time at pH higher than 4 is strongly supported by a gas evolution rate reduced with immersion time, as shown in Figure 1.

3.6. Surface Morphology

FESEM images of the AZ31 Mg alloy surface immersed for 30 min in sulfate-ion-containing aqueous solutions with different pHs are presented in Figure 8. Numerous scratches and second-phase particles were observed from the bare AZ31 Mg alloy surface (Figure 8a). At pH 2, the AZ31 Mg alloy surface showed very thick films with wide cracks, which are interconnected. Narrow cracks were also observed, which are branched from the wide cracks. The initial scratches disappeared after 30 min of immersion at pH 2, which indicates fast corrosion during immersion. Cracks in the AZ31 Mg alloy caused by corrosion were reported to occur due to the preferential galvanic dissolution of the Mg matrix surrounding the β-phase particles, primarily precipitating along the grain boundaries [35].

At pH 3~11, the scratches and second-phase particles were visible even after 30 min of immersion (Figure 8d,f,h,j,l). This means that the corrosion rate of the AZ31 Mg alloy is considerably low at pH 3~12 compared to that at pH 2. Needle-like surface films were formed at pH 3~11 and flake-like surface films were observed at pH 12 on the AZ31 Mg alloy surface after immersion for 30 min in sulfate ion-containing solutions. In our previous work, the needle-like and flake-like surface films were reported to be composed of mainly $Mg(OH)_2$ and a small amount of $MgSO_4$ in neutral aqueous solutions [29]. It was also reported that the flake-like surface films are formed due to the growth of surface film in a preferential direction [36].

The porous structures of the surface films formed on AZ31 Mg alloy at different pHs are shown in Figure 9. At pH 2, the surface films showed a highly porous nature (Figure 9a), while at pH 3~12, relatively less porous structures were observed. The porous nature of the surface film at pH 2 could potentially facilitate the migration of corrosive species and thereby exacerbate corrosion. Previous studies have reported the formation of nanoporous

flake-like $Mg(OH)_2$ films in NaCl solutions, as well as the permeation of Cl^- ions through both $Mg(OH)_2$ and MgO films, leading to corrosion [37].

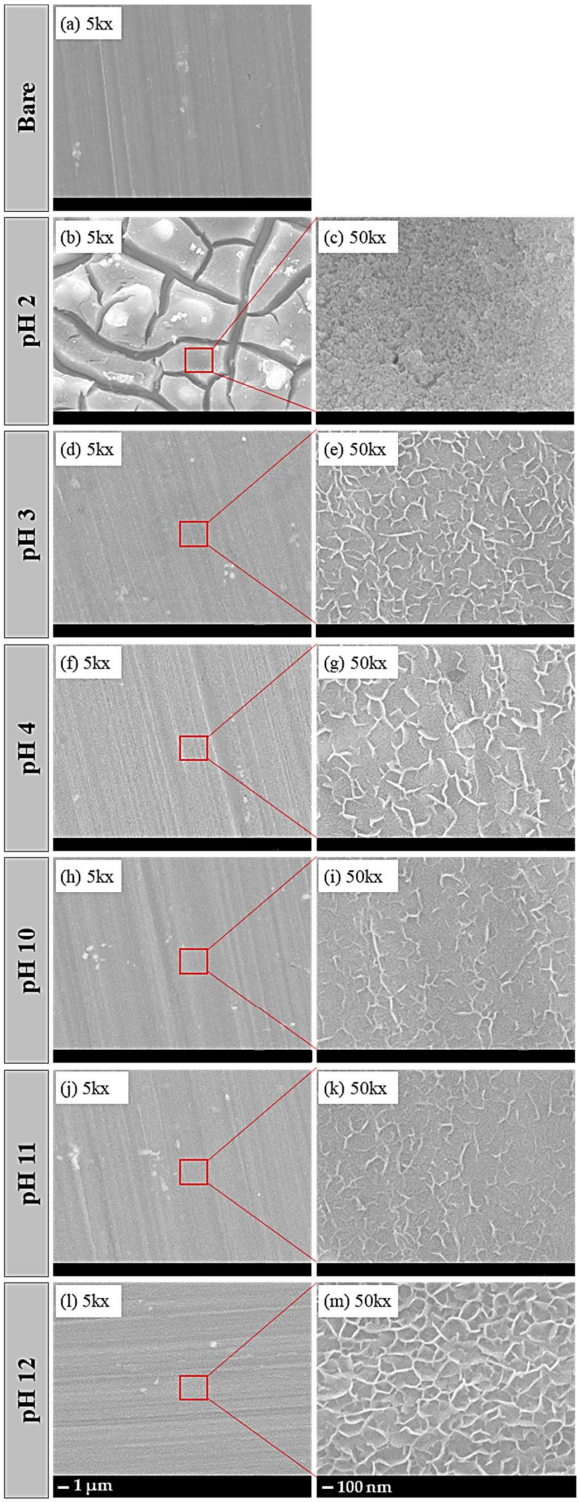

Figure 8. FESEM images of the AZ31 Mg alloy surface which were immersed for 30 min in sulfate-ion-containing aqueous solutions with different pHs.

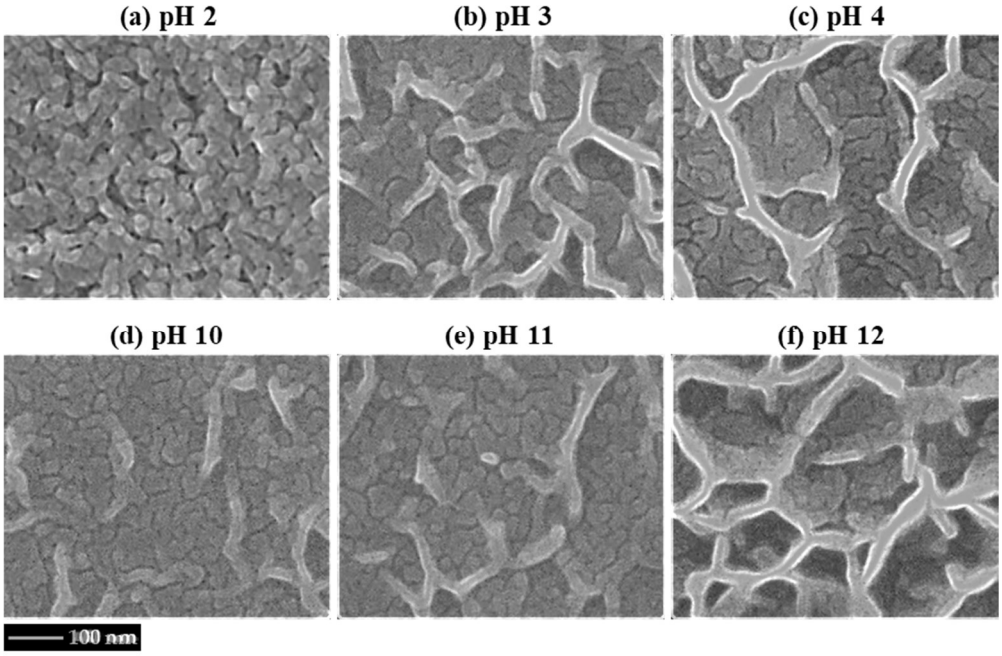

Figure 9. Magnified surface images of Figure 8c,e,g,i,k,m.

The extremely low impedance value in Figure 5 and high weight loss rate in Figure 4 should be related to the high porosity of surface films formed at pH 2. At pH 3~11, slightly porous surface films with nanopores were found around the needle-like structures (Figure 9b–e), while a comparatively less porous surface film was found on the flake-like surface (Figure 9m). It should be noted that a more porous surface film with low film resistance forms in aqueous solutions at low pHs, while at higher pHs, a relatively dense and protective surface film can be formed.

4. Conclusions

This study explores the corrosion and film formation behavior on AZ31 Mg alloy in sulfate-ion-containing aqueous solutions with different pHs ranging from 2 to 12. In the sulfate-ion-containing solution adjusted to pH 2, vigorous hydrogen evolution and corrosion occurred over the 30 min of immersion, showing a weight loss of -39.099 $\mu g/cm^2 \cdot min$, and highly porous surface films with a wide and narrow cracks were formed. At pH 3 of the sulfate-ion-containing aqueous solution, the corrosion rate of the AZ31 Mg alloy was greatly reduced, with a weight loss of -0.491 $\mu g/cm^2 \cdot min$. Extremely low corrosion rates of less than -0.165 $\mu g/cm^2 \cdot min$ and -0.126 $\mu g/cm^2 \cdot min$ were measured at pHs 4 and 10, respectively. Remarkably, the weight loss rate decreases by approximately 80 times as the pH of the aqueous solution changes from 2 to 3. In contrast, weight gains were found at pHs 11 and 12, which suggests the growth of surface films on the AZ31 Mg alloy with immersion time. Flake-like surface films were formed on the AZ31 Mg alloy surface at pH 12 and a needle-like structure of the surface films was obtained at pH 3~11. The impedance of the surface film increased significantly with increasing the pH of the sulfate-ion-containing aqueous solution in acidic solutions with a pH lower than 4, and alkaline solutions with a pH higher than 11. The high impedance values at high pHs are attributed to the formation of denser surface films on the AZ31 Mg alloy surface in alkaline solutions containing sulfate ions. MIM colors were observed at pHs higher than 4 in sulfate-ion-containing aqueous solutions, reflecting the uniform thickness of the surface films formed on the AZ31 Mg alloy surface, although these contain needle-like or flake-like structures.

Author Contributions: Conceptualization, D.K. and S.M.; investigation, D.K. and H.V.P.; writing—original draft preparation, D.K.; writing—review and editing, D.K., H.V.P., P.S. and S.M.; supervision, S.M and P.S. All authors have read and agreed to the published version of the manuscript.

Funding: This work was financially supported by the Fundamental Research Program of the Korean Institute of Materials Science (project no.: PNK9450).

Data Availability Statement: Not applicable.

Conflicts of Interest: The authors declare that they have no conflict of interest.

References

1. Xu, T.; Yang, Y.; Peng, X.; Song, J.; Pan, F. Overview of advancement and development trend on magnesium alloy. *J. Magnes. Alloys* **2019**, *7*, 536–544. [CrossRef]
2. Heimann, R.B. Magnesium alloys for biomedical application: Advanced corrosion control through surface coating. *Surf. Coat. Technol.* **2021**, *405*, 126521. [CrossRef]
3. Liu, B.; Yang, J.; Zhang, X.; Yang, Q.; Zhang, J.; Li, X. Development and application of magnesium alloy parts for automotive OEMs: A review. *J. Magnes. Alloys* **2023**, *11*, 15–47. [CrossRef]
4. Yan, P.; Ying, T.; Li, Y.; Li, D.; Cao, F.; Zeng, X.; Ding, W. A novel high corrosion-resistant polytetrafluoroethylene/carbon cloth/Ag coating on magnesium alloys as bipolar plates for light-weight proton exchange membrane fuel cells. *J. Power Sources* **2021**, *484*, 29231. [CrossRef]
5. Liu, H.; Cao, F.; Song, G.-L.; Zheng, D.; Shi, Z.; Dargusch, M.S.; Atrens, A. Review of the atmospheric corrosion of magnesium alloys. *J. Mater. Sci. Technol.* **2019**, *35*, 2003–2016. [CrossRef]
6. de Oliveira, M.C.L.; da Silva, R.M.P.; Souto, R.M.; Antunes, R.A. Investigating local corrosion processes of magnesium alloys with scanning probe electrochemical techniques: A review. *J. Magnes. Alloys* **2022**, *10*, 2997–3030. [CrossRef]
7. Zhao, D.; Jiang, C.; Zhao, K. Ultrasonic welding of AZ31B magnesium alloy and pure copper: Microstructure, mechanical properties and finite element analysis. *J. Mater. Res. Technol.* **2023**, *23*, 1273–1284. [CrossRef]
8. Zhang, Z.; Zhang, J.; Xie, J.; Liu, S.; Fu, W.; Wu, R. Developing a Mg alloy with ultrahigh room temperature ductility via grain boundary segregation and activation of non-basal slips. *Int. J. Plast.* **2023**, *162*, 103548. [CrossRef]
9. Xu, B.; Song, Y.; Yang, K.; Li, Y.; Chen, B.; Liao, X.; Jia, Q. Magnesium metal and its corrosion products: Promising materials for tumor interventional therapy. *J. Magnes. Alloys* **2023**, *11*, 763–775. [CrossRef]
10. Mitchell, J.; Crow, N.; Nieto, A. Effect of Surface Roughness on Pitting Corrosion of AZ31 Mg Alloy. *Metals* **2020**, *10*, 651. [CrossRef]
11. Cao, X.; Ren, Q.; Yang, Y.; Hou, X.; Yan, Y.; Hu, J.; Deng, H.; Yu, D.; Lan, W.; Pan, F. A new environmentally-friendly route to in situ form a high-corrosion-resistant nesquehonite film on pure magnesium. *RSC Adv.* **2020**, *10*, 35480–35489. [CrossRef] [PubMed]
12. Li, H.; Wen, J.; Liu, Y.; He, J.; Shi, H.; Tian, P. Progress in Research on Biodegradable Magnesium Alloys: A Review. *Adv. Eng. Mater.* **2020**, *22*, 2000213. [CrossRef]
13. Qu, Q.; Ma, J.; Wang, L.; Li, L.; Bai, W.; Ding, Z. Corrosion behaviour of AZ31B magnesium alloy in NaCl solutions saturated with CO_2. *Corrosion Sci.* **2011**, *53*, 1186–1193. [CrossRef]
14. Prince, L.; Rousseau, M.A.; Noirfalise, X.; Dangreau, L.; Coelho, L.B.; Olivier, M.G. Inhibitive effect of sodium carbonate on corrosion of AZ31 magnesium alloy in NaCl solution. *Corrosion Sci.* **2021**, *179*, 109131. [CrossRef]
15. Soltan, A.; Dargusch, M.S.; Shi, Z.; Gerrard, D.; Al Shabibi, S.; Kuo, Y.-C.; Atrens, A. Corrosion of Mg alloys EV31A, WE43B, and ZE41A in chloride- and sulfate-containing solutions saturated with magnesium hydroxide. *Mater. Corros.* **2020**, *71*, 956–979. [CrossRef]
16. Ge, F.; Cui, Z.; Liu, Y.; Lei, L.; Wang, X.; Cui, H. Influence of ammonium sulfate on the corrosion behavior of AZ31 magnesium alloy in chloride environment. *J. Magnes. Alloys* **2022**, in press. [CrossRef]
17. Liu, W.; Cao, F.; Xia, Y.; Chang, L.; Zhang, J. Localized Corrosion of Magnesium Alloys in NaCl Solutions Explored by Scanning Electrochemical Microscopy in Feedback Mode. *Electrochim. Acta* **2014**, *132*, 377–388. [CrossRef]
18. Feng, Z.; Li, J.; Yang, Z.; Buchheit, R. The Effect of Vanadate, Phosphate, Fluoride Compounds on the Aqueous Corrosion of Magnesium Alloy AZ31 in Dilute Chloride Solutions. *Materials* **2020**, *13*, 1325. [CrossRef]
19. Shen, J.; Lai, T.; Yin, Z.; Chen, Y.; Wang, K.; Yan, H.; Song, H.; Liu, R.; Luo, C.; Hu, Z. In-situ AFM and quasi-in-situ studies for localized corrosion in Mg-9Al-1Fe-(Gd) alloys under 3.5 wt.% NaCl environment. *J. Magnes. Alloys*, 2022; *in press*. [CrossRef]
20. Harrison, R.; Maradze, D.; Lyons, S.; Zheng, Y.; Liu, Y. Corrosion of magnesium and magnesium–calcium alloy in biologically-simulated environment. *Prog. Nat. Sci.* **2014**, *24*, 539–546. [CrossRef]
21. Cao, X.; Jia, Q.; Xu, C.; Zhang, Z.; Ren, C.; Yang, W.; Zhang, J. Research on Dynamic Corrosion Behavior and the Microstructure of Biomedical Mg–Y–Zn–Zr–Sr in Simulated Body Fluid Solution after Processing by Solution Treatment. *Adv. Eng. Mater.* **2020**, *22*, 1901146. [CrossRef]
22. Jiang, Q.; Lu, D.; Cheng, L.; Liu, N.; Yang, L.; Hou, B. The corrosion behavior of EW75 magnesium alloy in the research vessel KEXUE during the ocean voyage. *NPJ Mater. Degrad.* **2022**, *6*, 28. [CrossRef]
23. Samaniego, A.; Hurley, B.L.; Frankel, G.S. On the evidence for univalent Mg. *J. Electroanal. Chem.* **2015**, *737*, 123–128. [CrossRef]
24. Song, G.; Atrens, A. Understanding Magnesium Corrosion—A Framework for Improved Alloy Performance. *Adv. Eng. Mater.* **2003**, *5*, 837–858. [CrossRef]
25. Zhou, X.; Jiang, L.; Wu, P.; Sun, Y.; Yu, Y.; Wei, G.; Ge, H. Effect of aggressive ions on degradation of WE43 magnesium alloy in physiological environment. *Int. J. Electrochem. Sci.* **2014**, *9*, 304–314.

26. Kwon, D.; Pham, H.V.; Song, P.; Moon, S. Electrochemical behavior of AZ31 Mg alloy in neutral aqueous solutions containing various anions. *J. Electrochem. Sci. Technol.* 2023; *Epub ahead of print*. [CrossRef]
27. Kwon, D.; Pham, H.V.; Song, P.; Moon, S. Corrosion Behavior of the AZ31 Mg Alloy in Neutral Aqueous Solutions Containing Various Anions. *Metals* **2023**, *13*, 962. [CrossRef]
28. Huang, J.; Song, G.-L.; Atrens, A.; Dargusch, M. What activates the Mg surface—A comparison of Mg dissolution mechanisms. *J. Mater. Sci. Technol.* **2020**, *57*, 204–220. [CrossRef]
29. Yan, D.; Wang, Y.; Liu, J.; Song, D.; Zhang, T.; Liu, J.; He, F.; Zhang, M.; Wang, J. Self-healing system adapted to different pH environments for active corrosion protection of magnesium alloy. *J. Alloys Compd.* **2020**, *824*, 153918. [CrossRef]
30. Van Phuong, N.; Moon, S.; Chang, D.; Lee, K.H. Effect of microstructure on the zinc phosphate conversion coatings on magnesium alloy AZ91. *Appl. Surf. Sci.* **2013**, *264*, 70–78. [CrossRef]
31. Fazal, B.R.; Moon, S. Electrochemical Properties of Air-Formed Oxide Film-Covered AZ31 Mg Alloy in Aqueous Solutions Containing Various Anions. *J. Kor. Inst. Surf. Eng.* **2017**, *50*, 147–154. [CrossRef]
32. Yang, Q.; Chen, L.; Xu, J.; Gong, Y.; Deng, L.; Chen, C. Study of the Corrosion and Surface Film Growth on AZ63 Magnesium Alloy in $MgSO_4$ Solution. *J. Electrochem. Soc.* **2017**, *164*, C324. [CrossRef]
33. Yang, L.; Shi, X.; Tian, X.; Xue, Y.; Wang, J.; Qi, L. Influence of pH value on the microstructure and corrosion behavior of carbon fiber reinforced magnesium matrix composites. *J. Mater. Res. Technol.* **2022**, *17*, 412–424. [CrossRef]
34. Kim, Y.H.; Rahman, M.A.; Hwang, J.S.; Ko, H.; Huh, J.-Y.; Byun, J.Y. Reflection color tuning of a metal–insulator–metal cavity structure using arc plasma deposition of gold nanoparticles. *Appl. Surf. Sci.* **2021**, *562*, 150140. [CrossRef]
35. Merson, E.; Myagkikh, P.; Poluyanov, V.; Merson, D.; Vinogradov, A. On the role of hydrogen in stress corrosion cracking of magnesium and its alloys: Gas-analysis study. *Mater. Sci. Eng. A-Struct. Mater. Prop. Microstruct. Process.* **2019**, *748*, 337–346. [CrossRef]
36. Maltseva, A.; Shkirskiy, V.; Lefèvre, G.; Volovitch, P. Effect of pH on $Mg(OH)_2$ film evolution on corroding Mg by in situ kinetic Raman mapping (KRM). *Corrosion Sci.* **2019**, *153*, 272–282. [CrossRef]
37. Brady, M.P.; Rother, G.; Anovitz, L.M.; Littrell, K.C.; Unocic, K.A.; Elsentriecy, H.H.; Song, G.L.; Thomson, J.K.; Gallego, N.C.; Davis, B. Film Breakdown and Nano-Porous $Mg(OH)_2$ Formation from Corrosion of Magnesium Alloys in Salt Solutions. *J. Electrochem. Soc.* **2015**, *162*, C140. [CrossRef]